Yb_2O_3 Doped Yttrium-Alumino-Silicate Nano-Particles Based LMA Optical Fibers for High-Power Fiber Lasers

M. C. Paul, *Member, IEEE*, A. V. Kir'yanov, *Member, IEEE*, Yu. O. Barmenkov, *Member, IEEE*, S. Das, M. Pal, S. K. Bhadra, S. Yoo, A. J. Boyland, J. K. Sahu, A. Martínez-Gamez, and J. L. Lucio-Martínez

***Abstract*—Yb_2O_3 doped yttrium-rich alumino-silicate nano-particles based D- and P- (pentagonal) shaped optical fibers with core diameter ~30–35 μm are fabricated using the conventional MCVD process and solution doping technique. Parameters of different stages of the fiber preforms fabrication are optimized to get uniform distributions of Al, Y, F, and Yb ions in the core region, ensured by the data of an EPMA analysis. In the presence of small amounts of fluorine, the size of nano-particles is maintained within 5–10 nm; the EDX data reveal that the nano-particles are rich in yttrium-alumino-silicate phase and are dispersed uniformly across the preforms core. The critical parameters of the processes involved at the fibers fabrication along with the nano-structuring and spectroscopic features are highlighted. It is shown experimentally that the drawn D- and P- shaped fibers support high laser efficiency (~80% at 976-nm pumping) and demonstrate negligible photodarkening.**

***Index Terms*—Fiber optics, fiber lasers, nanoparticles.**

I. Introduction

CONSIDERABLE work was carried out on the incorporation of rare-earth (RE) oxide nano-particles into different glass hosts. A number of processes were inspected to solve the problem, such as co-sputtering technique [1], pyrolysis [2], ion implantation [3], laser ablation [4], sol-gel [5], and direct deposition [6]. However, when the target is the fabrication of RE doped optical fibers with nano-engineered core glass, the solution doping (SD) technique [7] in the modified chemical vapor deposition (MCVD) process seems to be the most natural. An example of synthesis of Er_2O_3 doped nano-particles-based calcium-germano-silicate glass for fiber applications using the basic principles of phase-separation phenomena was reported in [8].

Here we report, for the first time to the best of our knowledge, the incorporation of Yb_2O_3 into yttrium-alumino-silicate (YAS: Y_2O_3-Al_2O_3-SiO_2) phase-separated nano-particles into the core of large-mode-area (LMA) fibers with core diameter ~30–35 μm. This was done through the chemical impregnation of porous phospho-silicate deposited layers, using suitable strength of the doping precursors via the SD technique. The method allowed optimization of the fabrication process parameters for obtaining uniform doping through the whole core area of final fibers [9].

An important property of Y_2O_3 is that the dominant phonon energy of this sesquioxide is one of the smallest values of phonon cutoff energy among oxides (~377 cm^{-1} [10]; the other is ~550 cm^{-1} [11]), allowing mostly radiative transitions between the electronic levels of Yb_2O_3. Below, we report on fabricating and study of optical preforms and fibers with yttrium-rich Yb_2O_3 doped alumino-silicate core glass where the dominant portion of Ytterbium enters into the phase-separated nano-particles. Such fibers may have potential usage because of the highest known vibrational energy (YAS) host glass, ~950 cm^{-1} [12], which is less than maximal vibrational energy of silica glass (~1100 cm^{-1} [13]). The choice of Y and Al as co-dopants was done due to the same valence of Al^{3+}, Y^{3+}, and Yb^{3+} and similar lattice structures of Al_2O_3, Y_2O_3, and Yb_2O_3 oxides. We highlight below the critical fabrication parameters and the material characterization results together with the spectroscopic properties of final nano-particles based D- and P- (pentagonal) shaped LMA fibers. The results of laser tests are then presented, which demonstrate that overall optical efficiency at diode pumping at 976 nm is as high as 80% for these fibers at their negligible photodarkening.

II. Fabrication and Characterization of Fiber Preforms

Incorporation of Ytterbium into nano-engineered YAS based preforms was done through the MCVD process and SD technique followed by suitable thermal treatment of the preforms. At the first step, ten porous layers of SiO_2-P_2O_5 composition were deposited consecutively one after another at the optimum reaction temperature around $1240 \pm 10°C$ with flow of mixture of $SiCl_4$, $POCl_3$, O_2, and He into a rotating silica tube heated by an external H_2/O_2 burner that moves along the tube. Such SiO_2-P_2O_5 porous layers were deposited through the oxidation reaction of the vapor of $SiCl_4$ and $POCl_3$ with O_2. At this temperature, the chloride precursors oxidize, forming particles that

Manuscript received August 30, 2011; revised February 17, 2012, March 14, 2012; accepted March 14, 2012. Date of publication April 03, 2012; date of current version April 27, 2012. This work was supported in part by the Programme of Cooperation in Science and Technology between India and Mexico.

A. V. Kir'yanov, Yu. O. Barmenkov, and A. Martínez-Gamez are with the Centro de Investigaciones en Optica, Leon 37150, Guanajuato, Mexico (e-mail: kiryanov@cio.mx).

M. C. Paul, S. Das, M. Pal, and S. K. Bhadra are with the Fiber Optics and Photonic Division, Central Glass and Ceramic Research Institute-CSIR, Kolkata 700 032, India (e-mail: paulmukul@hotmail.com).

S. Yoo is with School of Electrical and Electronic Engineering, Nanyang Technological University, Singapore.

A. J. Boyland and J. K. Sahu are with the Optoelectronics Research Centre, University of Southampton SO17 1BJ, U.K.

J. L. Lucio-Martínez is with the Division de Ciencias e Ingenierías de la Universidad de Guanajuato, Leon 37150, Guanajuato, Mexico.

Color versions of one or more of the figures in this paper are available online at http://ieeexplore.ieee.org.

Digital Object Identifier 10.1109/JLT.2012.2191391

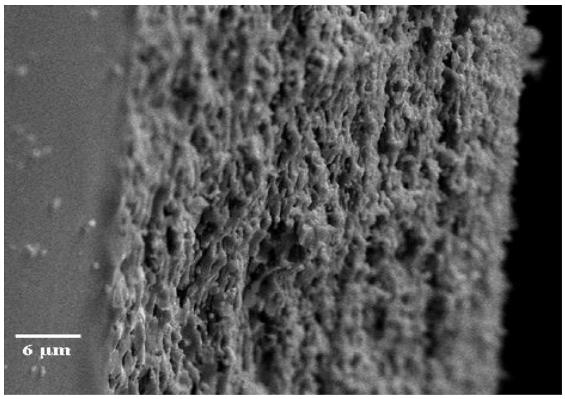

Fig. 1. Radial microscopic view of ten porous phospho-silicate layers.

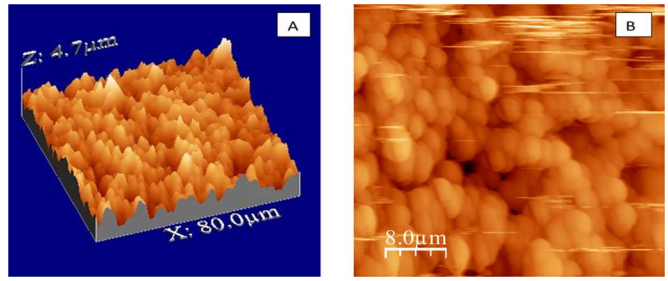

Fig. 2. (A) Three-dimensional and (B) cross-sectional AFM images of the surface of porous phospho-silicate multi-layers.

are deposited on the inner wall of the tube. Such kind of deposition is caused by thermophoresis, where suspended particles experience a net force in the direction of decreasing temperature, which is observed, in turn, due to a greater rate of collisions with gas molecules on the hot side of each particle that sinter together by viscous flow when the glass is sufficiently fluid.

After that, pre-sintering was fulfilled for three passes with gradually increasing temperature, from 1275 to 1300°C, for obtaining uniform porosity along both the axial and radial directions of thick (50–60 μm) layers. By this way, SiO_2 and P_2O_5 served as the glass formers incorporated through the vapor phase deposition process. Note that P_2O_5 was added into the deposited porous layers because this oxide also serves as a nucleating agent enhancing phase separation with generation of Yb_2O_3 doped micro- or nano-crystallites within the preform core area.

We used thin-wall silica tubes with inner diameter of 18 mm and cross-sectional area of 60 mm^2. The outer diameter was further enlarged to ~22.0 mm under optimum pressurization prior to deposition of multiple porous phospho-silicate layers. The purpose was to deposit thin individual layers (5.0–6.0 μm) for each deposition pass, which reduces the penetration length of the dissolved ions along the radial direction. Uniform soaking gave rise to uniform doping levels of the elements embedded in the whole core region as well as to a sharp refractive-index (RI) profile.

The techniques used for the analysis of porous silica layers were the scanning electron microscopy (SEM) and atom force microscopy (AFM). The SEM picture of 10 deposited porous layers along the radial direction is shown in Fig. 1.

The thickness of each layer was measured to be 5–6 μm. The three dimensional and cross-sectional images are shown in Fig. 2. Such three-dimensional and the corresponding cross-sectional images of the deposited porous surface show a hillock profile with a dome height of 3.0 ± 0.3 μm and the distance between the dome tops of 4 ± 1 μm (Fig. 2).

Both circular and irregular shaped pores with diameters of 3 ± 1 μm and the pore-to-pore distance of 4.5 ± 0.5 μm are seen here. The porosity of the deposited thick layers was found to be ~35%. In the second step, the silica tube with thick deposited porous layers was dipped into an alcoholic-water (1:5) mixture of appropriate strength of $YbCl_3 \cdot 6H_2O$, $AlCl_3 \cdot 6H_2O$, $YCl_3 \cdot 6H_2O$, and $LiNO_3$ for 40–45 minutes. After draining out of the solution, the layers were dried with flow of N_2 gas at room temperature. After air drying, a soaked layer containing Yb, Al, Y, and Li salts was heated at around 900–1000°C with flow of a mixture of O_2 (at the rate of 500 cc/min) and He (at the rate of 75–100 cc/min) for oxidation of the salts. By this way, the glass modifiers, Li_2O, Al_2O_3, Yb_2O_3, and Y_2O_3 were incorporated into the porous layers. Here Li_2O was used to increase optical transparency of the final doped glass.

After first solution soaking process, the silica tube with porous layers of SiO_2-P_2O_5-Y_2O_3-Al_2O_3-Yb_2O_3-Li_2O composition was dipped into H_2SiF_6 (fluorosilicic acid) for 15–20 minutes. Fluorine was incorporated into the porous layers through this second solution soaking process. To prevent etching of the porous layers in presence of fluorine, 10–15% diluted H_2SiF_6 was used. We have performed double solution soaking process to avoid the formation of gelatinous precipitation with a direct use of fluorosilic acid into the alcoholic solution of chloride precursors for fluorine incorporation.

After draining out of the fluorosilic acid, the layers were dried again by heating at 800–900°C. Incorporation of fluorine reduces RI of the core layer, maintaining its difference around 0.0025–0.003 when sufficient amounts of Yb_2O_3, Y_2O_3, and Al_2O_3 are added. After the oxidation step, porous layers were dehydrated at temperature 800–1100°C in the presence of Cl_2 and O_2, where the ratio Cl_2:O_2 was ranged from 1.5:1 to 3:1 for reducing the content of water. Sintering of the dehydrated porous layers was made with flow of a mixture of 80% O_2 and 20% He at temperatures ranged from 1300 to 1900°C with a step-wise increment by 100°C. At this step, fluorine was incorporated into the glass matrix. After complete sintering, the tube was collapsed, during 3 to 4 passes of the burner, with flow of a mixture of 90–95% O_2 and 10–5% He at temperatures between 2000 and 2300°C. The deposition of porous core layers, drying of soaked layers, sintering, and collapsing were fulfilled in highly oxidizing atmosphere to reduce the formation of any defects associated with aluminium oxygen-hole and Yb^{2+} centers.

After fabrication of fiber preforms, thermal annealing was done at 1450–1500°C for 3 hours in a controlled heating furnace at the heating and cooling rates of 20°C/min. At this step, Yb_2O_3 doped crystalline nano-particles were created in the core glass matrix; see Fig. 3, where the results of transmission electron microscopy (TEM), using the equipment Tecnai G^2 30ST, FEI Co, and electron diffraction measurements along with the EDX data are presented. The characteristic sizes of the nano-particles are seen to be 5 to 10 nm, see Fig. 3(A). The crystalline nature of nano-particles is clearly seen from inset (B) in Fig. 3, while the EDX spectra (Fig. 3(C)) show that these crystalline

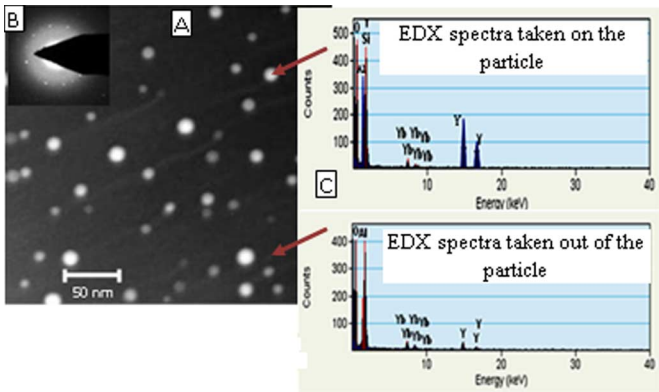

Fig. 3. (A) TEM micrograph along with (B) electron diffraction pattern within the core region of fiber preform section and (C) EDX spectra.

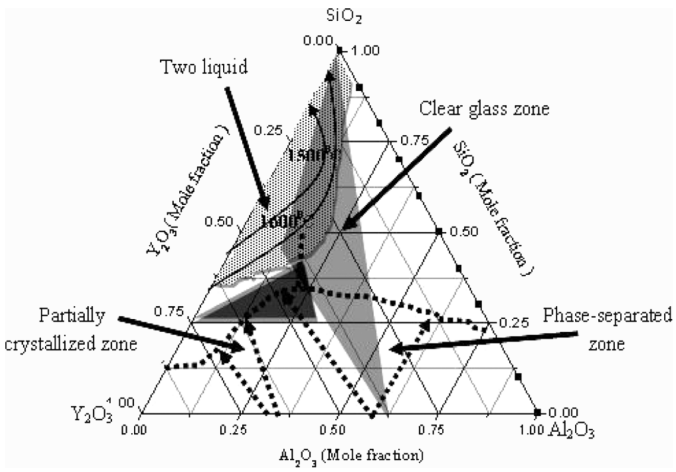

Fig. 4. Phase diagram of SiO_2-Al_2O_3-Y_2O_3 system derived from the FactSage software. Indicated are the partially crystallized, glass forming, and phase-separated zones of the glass.

particles are Yb_2O_3 doped yttria-alumino rich ones embedded into silica glass matrix.

The formation of phase-separated nano-particles starts when the ratio of Al:Y reaches $\sim$1.70–1.75 under suitable doping levels of Y_2O_3 and Al_2O_3 [14]. One of the reasons may be that YAS glass undergoes phase-separating once it "enters" the immiscible region. A ternary diagram of the YAS system is shown in Fig. 4, derived from the thermo-chemical software and database FactSage 5.5. The glass transition temperature of oxide glass is determined by a combination of several factors such as density of covalent cross-linking, number and strength of the coordinate links formed between oxygen and cation, and oxygen density of the network [15]. Such type of nano-structure is retained within the core glass matrix of optical fiber. Increasing the P_2O_5 content in the glass accelerates growth of formation of phase separated particles upon heating through thermal perturbation, where P_2O_5 serves as a nucleating agent owing to the higher field strength difference (>0.31) between Si^{4+} and P^{5+} [16]. Here, fluorine may also enhance the formation of phase-separated particles even at high temperature, around 1900–2000°C. On the other hand, the incorporation of P_2O_5 reduces photodarkening, an unwanted phenomenon known for Yb-doped high power fiber lasers.

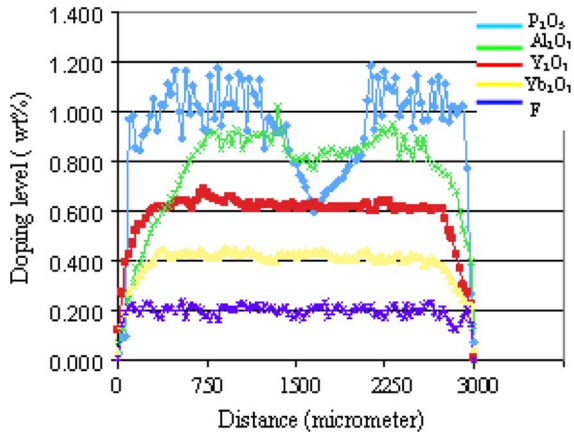

Fig. 5. Distributions of doping levels of the main dopants across the diameter of optical fiber preform IMNYb-12D, measured by EPMA.

The distributions of different doping elements within the core area of the fiber preforms determined from the EPMA measurements are shown in Fig. 5. All dopants are seen to be distributed uniformly along the whole core region.

After annealing of a preform, D- or P- shaping was done using the uniform grinding and polishing processes. Then, low RI coated fibers were drawn from the modified annealed D-(P-) shaped preforms, using a fiber drawing tower, at temperature around 2000°C. The nano-particles generated by this technique within the core region of optical fiber preform before and after thermal annealing process were analyzed in details earlier [14]. To create phase-separated particles in the core region, annealing of the preform sample is essential. It was observed that when the fiber is drawn from the preform without heat-treatment, nano-particles are not formed at all. For this reason, we used such kind of heat-treatment to generate phase-separated nano-particles within the fiber core, which permitted us to improve the lasing quality of final fibers and reduce photodarkening in them. Also notice that the incorporation of fluorine into the doping host was important since it reduces RI of silica glass (as the result, this helps in maintaining reduced RI difference, mentioned above) and results in decreasing the size of nano-particles and minimizing scattering in the fibers.

III. Characterization of Final Fibers

High-power applications of LMA fibers require cladding-pumping arrangements. The drawback of the double-clad fiber concept is the reduced pump light absorption per unit length. Some high-order pump modes existing in the inner cladding have small overlap with the doped Yb^{3+} core, which decreases the pump efficiency. Therefore, D- and P- shaped inner cladding structures are the most suitable to improve significantly pump absorption due to breaking of the cylindrical symmetry of the inner-clad, which leads to increasing an energy transfer between the pump modes.

The microscopic pictures of the fiber cross-sections were taken using an optical microscope. The cross-sectional views of D- and P- shaped LMA fibers (having diameters around 30 and 35 μm, respectively) are shown in Fig. 6.

The RI profiles of the fabricated fibers were measured by a Fiber Analyser. The RI profile of one of the fibers is shown in Fig. 7. The RI profile is very sharp at the core-cladding

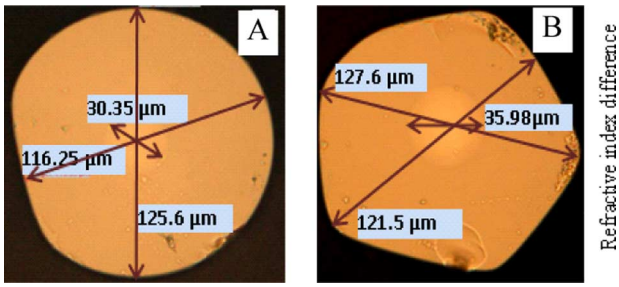

Fig. 6. Cross-sectional views of (A) D- (IMNYb-12D) and (B) P- (IMNYb-12P) shaped optical fibers.

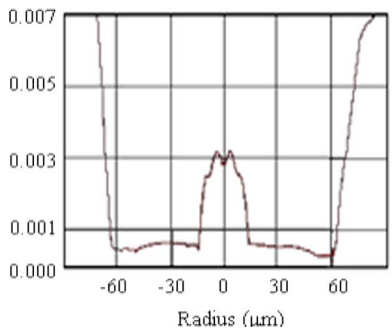

Fig. 7. RI profile of IMNYb-12D fiber.

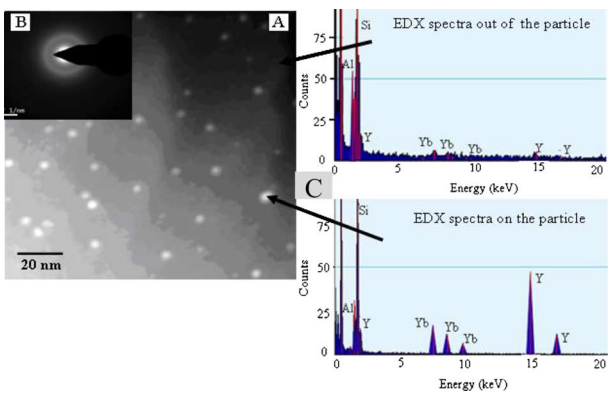

Fig. 8. TEM image (middle, A) and EDX curves (right, C), measured on and out of nano-particles. Inset (B) shows the electron diffraction pattern (the data for fiber IMNYb-12D).

boundary; it also demonstrates a dip at the core axis that arises due to evaporation of P_2O_5 from the central deposited layer during the collapsing stage. Sharpness of the RI profile indicates that the doping elements are embedded uniformly within the core region of the fiber.

The morphology of the core glass of bare optical fibers was studied by the TEM analysis and the nature and composition of nano-particles—by the electron diffraction and EDX analyses. The presence of nano-particles in final fibers was confirmed by the TEM measurements as shown in Fig. 8(A).

The size of nano-particles was found to be within the 5.0–10.0 nm range (see the bright spots in the TEM image which illustrate the phase-separated areas. The EDX spectra shown at the right side of Fig. 8(C) reveal that yttrium and ytterbium are dominant in the phase-separated particles but they are sparse in the non-phase-separated areas.

Furthermore, the peaks corresponding to aluminium in phase-separated particles is much lower than those in non-phase-separated region. Thus, we can conclude that majority of Ytterbium ions is located in the phase-separated yttria-rich region rather than in aluminium-dominated non-phase-separated areas. The nature of phase-separated particles was found to be non-crystalline, confirmed by their electron diffraction pattern, shown in inset (B) to Fig. 8. Diffuse scattering in the electron diffraction pattern (a "halo") reveals the amorphous nature of the particles, since there is not any diffraction spot in it. In this sense, the particles in the final fibers can be named "dielectric nano-particles" (DNPs), because the crystalline properties of the particles which were present in the start preforms are lost.

The sizes of the particles are found to be the same both at the preform and fiber stages (compare Fig. 8 with Fig. 3 above). This could be explained by the fact that Y_2O_3 serves as the host refractory oxide with a melting point of 2380°C. As a result, at the fiber drawing temperature (2000°C), only small changes in the sizes of particles from the preform to the final fiber are observed. At the preform stage, the shape of most of nano-particles is spherical. On the other hand, at the fiber stage, the shapes of some particles become non-spherical: They are elongated during the drawing process.

In the meantime, the contents of Yb, Al, and Y ions per a particle in the preform core, derived from the EDX spectra shown in Fig. 3, are larger than those in the fiber core, estimated from the EDX spectra (Fig. 8). This indicates that the materials in the particles in the preform core started to be incorporated into the surrounding glass during the fiber drawing stage.

The Yb-doped fibers were then investigated through a set of characterization procedures that included the measurements of absorption and fluorescence spectra, using an optical spectrum analyzer, as well as the measurements of fluorescence lifetimes. Finally, an analysis of the resultant fibers in the sense of laser properties was performed.

The absorption spectra were measured applying a standard cut-back procedure using a white-light source while Yb fluorescence spectra and fluorescence kinetics were obtained upon in-core pumping of the fibers by a diode laser with single-mode fiber output (300 mW; 978 nm) in the lateral detecting arrangement. The laser experiments were performed using a 976-nm multimode pump laser that was built on a set of diode arrays and a pump combiner, thus providing the clad-pump configuration. The examples of optical absorption and fluorescence of final Yb_2O_3 doped DNPs based LMA fibers are shown in Figs. 9–11. It is seen that the absorption spectra (Fig. 9) are quite similar in the appearance for both fibers, differing only in extinction within the Yb^{3+} peaks. Compared to a standard Yb-doped alumino-silicate fibers, these spectra are peculiar in presence of a wide attenuation background band that extends from near-IR to VIS. We attribute this background loss to the presence of yttria-rich DNPs in the core glass, the feature that resembles the appearance of specific bands known for Si nano-particles in silica fibers [17]. Notice that this extra attenuation that partially matches the resonant Yb^{3+} peaks didn't result in any worsening of laser properties of the fibers (see below, Fig. 14).

The background loss of both D- and P- shaped Yb-doped DNPs based LMA fibers was additionally verified using a high-resolution optical time-domain reflectometer (OTDR, Luciol). The background loss at 1285 nm was found to be

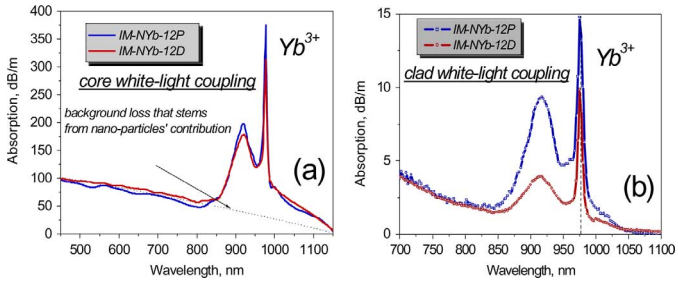

Fig. 9. Absorption spectra of D- (IMNYb-12D) and P- (IMNYb-12P) shaped fibers: (a) Core white light coupling and (b) Clad white light coupling.

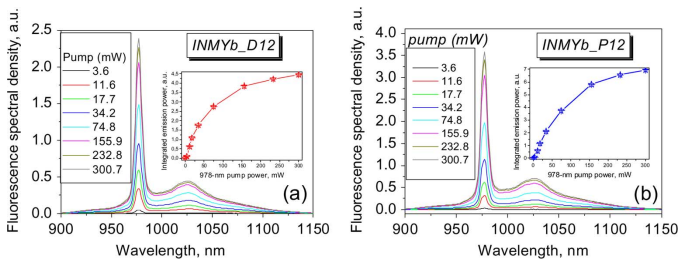

Fig. 10. NIR fluorescence spectra of (a) D- (IMNYb-12D) and (b) P- (IMNYb-12P) shaped fibers at in-core 976-nm excitation. Insets demonstrate integrated emission powers within ytterbium resonant band.

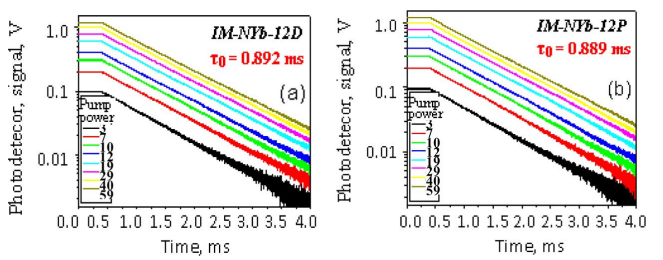

Fig. 11. Fluorescence lifetime decay of (a) D- (IMNYb-12D) and (b) P- (IMNYb-12P) shaped fibers at in-core 976-nm excitation.

40–400 dB/km, depending on the core composition and the size of DNPs.

The absorption spectra in Fig. 9(a) were measured at launching white light in-core. The absorption coefficients within the resonant-absorption peaks of Yb^{3+} as well as the non-resonant attenuation, most probably stemming from the presence of scattering DNPs, cannot be taken for a proper comparison with the laser experiments, where cladding multimode pumping of the fibers was used. The values of absorption coefficient at 976-nm peak of Ytterbium are ~350–400 dB/m at core-pumping (Fig. 9(a)) and ~10–15 dB/m at clad-pumping (Fig. 9(b)), respectively. Assuming homogeneous distributions of Yb^{3+} ions, dissolved in the glass network (with a filling factor ~90–95%) and presented in DNPs (with a filling factor ~5–10%) (see left part of Fig. 8), taking into account that the Yb signal from nano-particles is 4–5 times stronger than that from outside (see right part of Fig. 8), and implying that the absorption cross section of Yb^{3+} in alumino-silicate glass is around $(2–3) \times 10^{-20}$ cm^2 [18], we can estimate average concentration of Yb^{3+} ions in the fiber core as $\sim 1 \times 10^{18}$ cm^{-3} (~300 weight ppm), with the partial contributions being $\sim 0.8 \times 10^{18}$ cm^{-3} for the Yb^{3+} ions dissolved in glass matrix and $\sim 3.5 \times 10^{18}$ cm^{-3} (1050 weight ppm) for the Yb^{3+} ions entering DNPs.

The measurements of Yb^{3+} fluorescence spectra and lifetimes were performed in the lateral configuration where a fiber sample of a few cm in length was in-core pumped and the emission signal was collected from its lateral side, using a multimode patch-cord connected with an OSA, or using a fast photo-detector. We employed for in-core pumping a standard laser diode (LD) with single-mode fiber output of 300 mW. The LD output fiber was spliced to a tested Yb-doped fiber that was angle-cleaved from the other side. In the case of lifetime measurements, LD was modulated by a rectangular signal, producing square-shaped pump pulses of ms-width with sharp rise and fall edges. The time resolution of the setup was ~8 μs.

The fluorescence spectra within the spectral range where Yb^{3+} resonant peaks are located are shown in Fig. 10(a),(b) for the fiber samples with D- and P- shape, respectively.

It is seen from Fig. 10 that fluorescence spectra of the fibers are quite similar to those of standard alumino-silicate Yb-doped fibers. Furthermore, the fibers are characterized by quite low saturating pump power at 978-nm wavelength (~30 mW), which is important for the laser/amplifying applications.

Fig. 11(a),(b) shows the measured fluorescence decays found for DNPs based fibers having D- and P- shape. Fiber lengths less than 5 cm were used in these experiments to diminish a contribution of unwanted amplified spontaneous emission (ASE); the fluorescence signal was collected from the lateral surface of a fiber sample at the point separated by approximately 5 mm from its splice with the LD output fiber. We have fulfilled the lifetime measurements for both fibers at comparatively low pump powers (up to 70 mW), for ensuring the absence of any artifacts.

It is seen that both fibers demonstrate virtually single-exponential fluorescence decay, with a time constant being 0.89 ± 0.01 ms; see Fig. 11. These values are comparable with those known for standard alumino-silicate nano-particles free Yb-doped fibers.

The results of laser experiments with the fabricated fibers are highlighted by Figs. 12–14. In a preliminary test, D-shaped DNPs based Yb-doped fiber was placed into Fabry–Perot non-resonant cavity composed by two fiber cuts on the cavity opposite sides. The spectra of free-running laser operation were captured using an OSA. It was found that both the laser wavelength and laser line bandwidth depend on pump power. Fig. 12 represents CW laser spectra (resolution of OSA was turned to 0.2 nm). Under pump power of 15 W, the fiber laser shows a broadband oscillation between 1052 and 1085 nm.

When pump power was increased to 25 W (maximum), the starting output spectrum shifted to longer wavelength showing broadband oscillation between 1058 and 1085 nm. We can propose that such kind of free-run lasing may arise from the presence of two sorts of Ytterbium ions having different surrounding environment, the first ones being located within the yttria-rich DNPs while the second ones—in aluminium-rich phase outside DNPs. On the other hand, one cannot exclude somewhat different mechanisms for this spectral behavior of the laser, say, heating of an Yb-doped fiber at increasing pump power, which could result in shifting of generation spectrum to a longer wavelength—see e.g., [19], [20].

The main-course experiments, for revealing laser potential of the fabricated D- and P- shaped DNPs based Yb-doped LMA

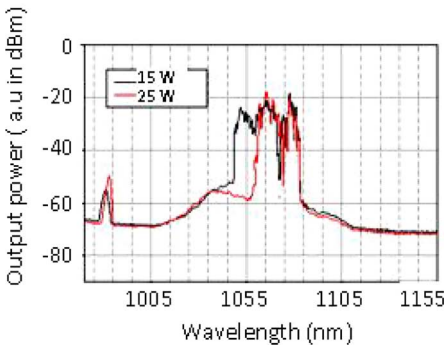

Fig. 12. Output spectrum of the lasing band of IMNYb-D12 fiber at pump power of 15W and 25W, respectively, launched from 976-nm laser-diode arrays.

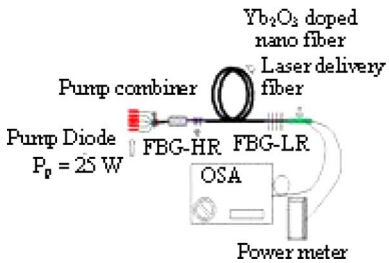

Fig. 13. Experimental setup for laser tests.

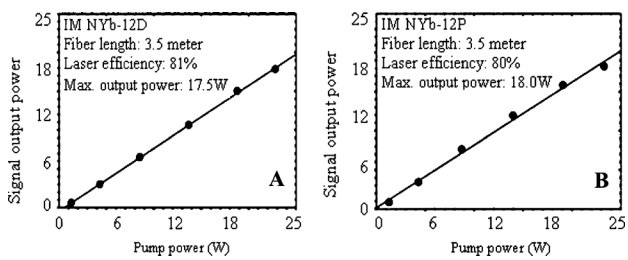

Fig. 14. Output power against absorbed pump power of fiber lasers based on (A) D-shaped IMNYb-12D and (B) P-shaped INMYb-12P fibers, both pumped at 976-nm wavelength.

fibers, were made using a setup sketched in Fig. 13. To explain the experimental results on lasing, we have measured the absorption spectra at in-clad launching of white light; see Fig. 9(b). A direct comparison of Figs. 9(a) and (b) permitted us to estimate the pump overlap factors that show effective coupling of pump light at 976 nm from cladding to core area, doped with Ytterbium. These factors were found for fibers 12D (D-shape) and 12P (P-shape) to be $\sim$0.03 and $\sim$0.04, respectively. So, in the last case the efficiency of clad-pumping is slightly better, which is in accordance with the results of laser experiments shown below in Fig. 14.

The fiber laser was pumped by a multimode fiber-coupled laser diode stack operating at 976-nm wavelength through a fiber combiner. The laser cavity was formed by two fiber Bragg gratings (FBGs) with reflectivity 99% (HR) and 10% (LR) and both centered at 1080 nm, which were spliced directly with an Yb-doped fiber. The output characteristics of the lasers with the active fiber having D- and P- shape are highlighted by Fig. 14(a),(b).

It is seen that both lasers release around 18 W of CW power at 1080-nm wavelength (at pump power of 23 W) and remarkably high optical efficiency, in excess of 80%, one of the highest values accessible to-date using Yb-doped fibers. It is of mention that output power of the lasers was almost not subjected to degradation at long-term (hours) tests, revealing a negligible photodarkening effect in these new Yb_2O_3 doped DNPs based optical fibers, which is one of their important advantages. The results of photodarkening measurements were obtained, applying the procedures described in detail in [21]. The reduction of photodarkening in such-type of nano-engineered glass based fibers was already reported in our earlier work [22], where the photodarkening-induced loss was reduced by $\sim$20 times relatively to standard Yb-doped alumino-silicate fibers.

There are evidences for that the photodarkening process be associated with non-binding oxygen near surfaces of Ytterbium/Aluminium clusters that can be formed in silica materials co-doped with Yb^{3+} and Al^{3+}. The non-binding oxygen originates from Yb^{3+} substituting Si^{4+} sites. When subjecting Ytterbium to 976-nm pump radiation, excess energy is radiated as phonons, which causes a lone electron of a non-binding oxygen atom to shift to a nearest neighbor non-binding oxygen atom with creation of a hole and a pair of lone electrons, resulting in a Coulomb field between the oxygen atoms to form an unstable color center. The conversion of such unstable color center to a semi-stable center requires the shifting of one electron of the lone electron pair to the nearest neighbor site [23]. In YAS glass matrix, Yttrium (Y^{3+}) is chosen as a co-doping ion since its ionic radius is similar to the one of Yb^{3+} (0.0892 nm for Y^{3+} and 0.0985 nm for Yb^{3+}). Yb^{3+} and Y^{3+} have also the same valence; therefore they can easily substitute each other and can increase the distance between two Yb^{3+} ions within yttria-alumino-rich DNPs. In the case of co-doping with Yb^{3+} and Y^{3+}, the formation of Yb-O-Y-O-Yb may take place like at the formation of Er-O-Y-O-Er [24]. As a result of this, the formation of Yb-related ODC (Yb-Yb) can be diminished or even prevented. Hence, photodarkening may be reduced in such kind of DNPs based fibers. On the other hand, photodarkening in the Yb-doped alumino-silicate fibers may take place through the breaking of ODCs under the two-photon absorption that gives rise to release of free electrons. The released electrons may be trapped at Al or Yb sites and therefore may form a color center resulting in photodarkening. As the field strength of the modifying cation increases, either through decreasing ionic radius or increasing charge, it is expected a perturbation of the alumino-silicate network, because of the energetic stabilization provided by closer association of negatively charged species, in particular non-bridging oxygen. In YAS glass, increasing the Y/Si ratio should provide a smaller shielding of the Si nucleus because of the substitution of Al by Y, which may be related to the conversion of bridging oxygen to non-bridging oxygen [25].

Another possible reason of photodarkening is related with Y^{3+} ions that promote the conversion of AlO_4 groups to higher-coordinate species [26]. These species provide more oxygen surrounding spaces, thus reducing the number of ODCs, the hypothesized precursor to photodarkening. We believe that these arguments bring more clarity in understanding of why photodarkening in the new Yb-doped DNPs based fibers is very small;

however further experiments are definitively needed to confirm these ideas.

The role of such nano-particles can be explained by the following ways:

The presence of yttria-rich phase-separated nano-engineered host strongly modifies the surrounding environment of Yb^{3+} ions, which also, in the main part, form the nano-particles. This is expected to increase the electric dipole moment of the radiative transitions for getting high quantum efficiency of lasing. Slope efficiency exceeding 80% is only a confirmation that our fibers are competitive with the best Yb-doped fibers in the sense of lasing properties;

Most of Yb^{3+} ions is present in yttria rich alumino-silica phase-separated nano-particles where Y_2O_3 serves as attractive host for laser applications since it reduces the phonon energy of nano-particles (the dominant phonon energy of Y_2O_3 decreases down to 377 cm^{-1}, one of the smallest phonon cutoff energies among oxides [10]). Yb^{3+} ions embedded into the glass matrix based on the low-phonon energy nano-particles seem to be also responsible for spectral broadening of lasing.

Y_2O_3 possesses very high thermal conductivity (27 W/mK) [27] compared to other conventional dopants in silica glass matrix. The presence of nano-particles increases the surface area of Yb_2O_3 doped phase-separated glass as compared to conventional Yb_2O_3 doped glasses. Hence, such kind of nano-engineered glass based optical fibers may improve the heat dissimilation property of the host under the high pump powers. As a result, efficiency of lasing as well as beam quality of a fiber laser based on such material can be improved.

IV. Conclusion

In this paper, we reported on investigation of Yb_2O_3 doped YAS glass D- and P- shaped optical fibers with DNPs, having the core diameter around 30–35 μm. The fibers were fabricated through the conventional MCVD and SD techniques. We achieved almost uniform distributions of the doping elements in the core region of optical fiber preforms, using deposition of multiple porous phospho-silicate layers at optimum temperature with uniform porosity. The solution strength was managed to provide Yb_2O_3 doped phase-separated YAS DNPs within the core area of final optical fibers. To reduce the particles size, fluorine was incorporated under double solution soaking process of the layers. It was found that the crystalline nature of nanoparticles observed in start preforms is lost in final fibers, which become DNPs. Such DNPs based Yb-doped optical LMA fibers, D- or P- shaped, were inspected from the viewpoints of spectroscopy and laser properties. Laser tests demonstrated that the fibers permit reaching high laser efficiency, of around 80% at 976-nm multimode clad-pumping, and negligible photodarkening.

References

[1] M. Fujii, M. Yoshida, S. Hayashi, and D. K. Yamamoto, "Photoluminescence from SiO_2 films containing Si nanocrystals and Er: effects of nanocrystalline size on the photoluminescence efficiency of Er^{3+}," *J. Appl. Phys.*, vol. 84, no. 8, pp. 4525–4531, Oct. 1998.

[2] J. St. John, J. L. Coffer, Y. Chen, and R. F. Pinizzotto, "Synthesis and characterization of discrete luminescent erbium-doped silicon nanocrystals," *J. Am. Chem. Soc.*, vol. 121, no. 9, pp. 1888–1892, Mar. 1999.

[3] C. E. Chryssou, A. J. Kenyon, T. S. Iwayama, C. W. Pitt, and D. E. Hole, "Evidence of energy coupling between Si nanocrystals and Er^{3+} in ion-implanted silica thin films," *Appl. Phys. Lett.*, vol. 75, no. 14, pp. 2011–2013, Oct. 1999.

[4] W. T. Nichols, J. W. Keto, D. E. Henneke, J. R. Brock, G. Malyavanatham, M. F. Becker, and H. D. Glicksman, "Large-scale production of nanocrystals by laser ablation of microparticles in a flowing aerosol," *Appl. Phys. Lett.*, vol. 78, no. 8, pp. 1128–1130, Feb. 2001.

[5] E. M. Yeatman, M. M. Ahmad, O. McCarthy, A. Martucci, and M. Guglielmi, "Sol-gel fabrication of rare-earth doped photonic components," *J. Sol-Gel Sci. Technol.*, vol. 19, no. 1-3, pp. 231–236, Dec. 2000.

[6] M. Rajala, K. Janka, and P. Kykkänen, "An industrial method for nanoparticle synthesis with a wide range of compositions," *Rev. Adv. Mater. Sci.*, vol. 5, pp. 493–499, 2003.

[7] J. E. Townsend, S. B. Poole, and D. N. Payne, "Solution-doping technique for fabrication of rare-earth-doped optical fibers," *Electron. Lett.*, vol. 23, no. 7, pp. 329–331, Mar. 1987.

[8] W. Blanc, B. Dussardier, and M. C. Paul, "Er doped oxide nanoparticles in silica based optical fibres," *Glass Technol.—Eur. J. Glass Sci. Technol. A*, vol. 50, no. 1, pp. 79–81, Feb. 2009.

[9] M. C. Paul, B. N. Upadhyaya, S. Das, A. Dhar, M. Pal, S. Kher, K. Dasgupta, S. K. Bhadra, and R. Sen, "Study of the fabrication parameters of large core Yb_2O_3 doped optical fibre through solution doping technique," *Opt. Commun.*, vol. 283, no. 6, pp. 1039–1046, Mar. 2010.

[10] L. A. Riseberg, *The Relevance of Nonradiative Transitions to Solid State Lasers*. New York: Plenum Press, 1980.

[11] A. Ubaldini and M. M. Carnasciali, "Raman characterisation of powder of cubic RE_2O_3 (RE = Nd, Gd, Ddy, Tm, and Lu), Sc_2O_3 and Y_2O_3," *J. Alloys Compounds*, vol. 374–378, no. 1–2, pp. 374–378, Apr. 2008.

[12] P. Jander and W. S. Brocklesby, "Spectroscopy of yttria-alumina-silica glass doped with thulium and erbium," *IEEE. J. Quantum Electron.*, vol. 40, no. 5, pp. 509–512, May 2004.

[13] , M. Tomozawa and R. H. Doremus, Eds., *Glass I: Interaction With Electromagnetic Radiation*. New York: Academic, 1978, vol. 12, pp. 5–89.

[14] M. C. Paul, S. Bysakh, S. Das, S. K. Bhadra, M. Pal, S. Yoo, M. P. Kalita, A. J. Boyland, and J. K. Sahu, "Yb_2O_3 doped YAG nano-crystallites in silica based core glass matrix of optical fiber preform," *Mater. Sci. Eng. B*, vol. 175, pp. 108–119, 2010.

[15] N. H. Ray, "Composition-property relationships in inorganic oxide glasses," *J. Non-Cryst. Solids*, vol. 15, no. 3, pp. 423–434, 1974.

[16] , M. Tomazawa and R. H. Doremus, Eds., *Phase Separation in Glass*. New York: Academic, 1979, vol. 17, p. 71.

[17] P. R. Watekar, S. Moon, A. Lin, S. Ju, and W.-T. Han, "Linear and nonlinear optical properties of Si nanoparticles/Er-ions doped optical fiber," *J. Lightw. Technol.*, vol. 27, no. 5-8, pp. 568–575, Mar.–Apr. 2009.

[18] P. Barua, E. H. Sekiya, K. Saito, and A. J. Ikushima, "Influences of Yb^{3+} concentration on the spectroscopic properties of silica glass," *J. Non-Cryst. Sol.*, vol. 354, pp. 4760–4764, 2008.

[19] T. C. Newell, P. Peterson, A. Gavrieldes, and M. P. Sharma, "Temperature effects on the emission properties of Yb-doped optical fibers," *Opt. Commun.*, vol. 273, no. 1, pp. 256–259, May 2007.

[20] A. S. Kurkov, V. S. Paramonov, and O. I. Medvedkov, "Ytterbium fiber laser emitting at 1160 nm," *Laser Phys. Lett.*, vol. 3, no. 10, pp. 503–506, Oct. 2006.

[21] A. D. Guzman-Chavez, A. V. Kir'yanov, Yu. O. Barmenkov, and N. N. Il'ichev, "Reversible photo-darkening and resonant photobleaching of ytterbium-doped silica fiber at in-core 977-nm and 543-nm irradiation," *Laser Phys. Lett.*, vol. 4, no. 10, pp. 734–739, Oct. 2007.

[22] S. Yoo, M. P. Kalita, A. J. Boyland, A. S. Webb, R. J. Standish, J. K. Sahu, M. C. Paul, S. Das, S. K. Bhadra, and M. Pal, "Ytterbium-doped Y_2O_3 nanoparticle silica optical fibers for high power fiber lasers with suppressed photodarkening," *Opt. Commun.*, vol. 283, pp. 3423–3427, 2010.

[23] K. E. Mattsson, S. N. Knudsen, B. Cadier, and T. Robin, "Photo darkening in ytterbium co-doped silica material," in *Proc. SPIE*, 2008, vol. 6873, art. no. 68731C.

[24] T. N. Haa, P. N. Thanga, L. N. Chunga, P. T. Ngaa, Ph. V. Hoia, L. V. Luatb, T. Th. Chama, V. Th. K. Lienc, C. Barthoud, and P. Benallould, in *Proc. Int. Workshop Photon. Appl.*, Hanoi, Vietnam, Apr. 5–8, 2004, p. 147.

[25] T. Schaller and J. F. Stebbins, "The structural role of lanthanum and yttrium in aluminosilicate glasses: A Al-27 and O-17 MAS NMR study," *J. Phys. Chem. B*, vol. 102, no. 52, pp. 10690–10697, Dec. 1998.

[26] J. T. Kohli, J. E. Shelby, and J. S. Frye, "A structural investigation of yttrium aluminosilicate glasses using Si-29 and Al-27 magic angle spinning nuclear-magnetic-resonance," *Phys. Chem. Glasses*, vol. 33, no. 3, pp. 73–78, Jun. 1992.

[27] A. A. Kaminskii, *Laser Crystals*. Berlin, Germany: Springer, 1990.

Author biographies not included at authors' request due to space constraints.